Journal of Nuclear Materials 632 (2026) 156877

Contents lists available at ScienceDirect

Journal of Nuclear Materials

journal homepage: www.elsevier.com/locate/jnucmat

Effect of heating rate up to 300 K/min on high-temperature steam oxidation and degradation of Cr-coated Zry-4

Diana Bachurina *, Jaeyoon Bae, Ulrike Stegmeier, Martin Steinbrueck

Karlsruhe Institute of Technology Eggenstein-Leopoldshafen, Germany

ARTICLE INFO

Keywords:
ATF fuel
Cr-coating
Zirconium alloy
Severe accident
Steam oxidation

ABSTRACT

This work focuses on the oxidation performance of chromium-coated Zircaloy cladding under varying heating rates up to 1500 °C. Zircaloy-4 tubes, 12 cm in length and coated with 15 μm PVD-Cr, were tested in the QUENCH-SR facility. Oxidation of the cladding was conducted at heating rates between 5 and 300 K/min in steam. Hydrogen production was measured simultaneously, and post-test examinations included microstructural analysis. Increasing the heating rate primarily affects the microstructure by reducing oxidation time, resulting in thinner oxide layers, a finer eutectic microstructure, and the presence of residual Cr at 300 K/min. Although accelerated oxidation occurs above the eutectic temperature and the oxidation rate increases with heating rate, the total hydrogen production decreases. Under conditions relevant to severe accidents, Cr-coated samples release less hydrogen than uncoated Zircaloy-4.

1. Introduction

The Fukushima accident pushed the nuclear community to the extensive development of so-called accident-tolerant fuel (ATF), that can experience lower rates of high-temperature oxidation and produce less hazardous hydrogen in this process [1]. There are many concepts being developed, with the most promising being Cr-coated zirconium claddings [2–4], FeCrAl alloys [5,6] or SiC claddings [7,8]. The former has done its further development and is close to deployment. However, there are still many open questions regarding its behaviour in different accidental scenarios.

One of them is the behaviour when the temperature of the cladding exceeds 1330 °C, which is the eutectic temperature in the Cr-Zr system. Many researchers have investigated the eutectic reaction between Zr and Cr at high-temperature [9–14]. This reaction leads to the formation of a liquid phase at 1330 °C, which is lower than the melting point of Zr (1885 °C). When the eutectic reaction occurs, ridges form on the surface of the Zr alloy, which is visible to the naked eye and is called a "crocodile" skin. After this reaction occurs, the protectiveness of the coating is lost. It has been reported that Cr-coated Zry-4, after losing its protective coating, temporarily undergoes oxidation more severely than uncoated Zr alloy [9,12].

Previously, we analysed the oxidation behaviour in the heating range of 2–50 K/min using TGA equipment in oxygen with small sample plates [9]. It was shown that increasing the heating rate also increases the oxidation rate and the associated heat generation. At a heating rate of 50 K/min, the heat produced by oxidation may even exceed the decay heat after shutdown. Furthermore, the weight gain observed at 50 K/min was greater than that at lower heating rates, despite the shorter overall exposure time.

Liu et al. [15] investigated the oxidation of sheet samples of chromium-coated Zircaloy-4 heated up to 1600 °C at 10 K/min in steam. They demonstrated that, up to 1500 °C, Cr-coated samples produced totally less hydrogen than uncoated samples. However, once the eutectic temperature was reached, the oxidation rates exceeded those of the uncoated material. The authors also noted that the observed mechanisms should be further validated through experiments performed at higher heating rates.

In [16], the authors investigated cold-spray-coated claddings heated at 10 K/min in steam. An increase in hydrogen production was already observed at 1250 °C and subsequently exceeded the oxidation rate of uncoated samples above the eutectic temperature (approximately 1450 °C in that study). This phenomenon may become even more pronounced at higher heating rates.

Joung et al. [17] investigated PVD (physical vapour deposition) Cr-coated claddings heated up to 1400 °C in a steam environment under simulated extended LOCA conditions followed by quenching. They showed that the cladding neither fractured nor collapsed after testing.

* Corresponding author.
E-mail address: diana.bachurina@kit.edu (D. Bachurina).

https://doi.org/10.1016/j.jnucmat.2026.156877
Received 16 March 2026; Received in revised form 12 June 2026; Accepted 30 June 2026
Available online 30 June 2026

However, they concluded that embrittlement caused by the eutectic reaction plays a more critical role in cladding integrity than melting itself. Oxidation rates and hydrogen release, however, were not investigated in that study.

Apart from these studies, no other data is currently available for transient oxidation under different heating rates [3]. Most existing research focuses on isothermal conditions [18–28], while one study [28] also investigates transient oxidation terminated at temperatures below the eutectic reaction.

However, the real conditions differ from those at laboratory scale, particularly with respect to one-sided oxidation, transient conditions and heating rates which can reach 600 K/min. This study complements the TGA study in oxygen [9] and aims to examine the effect of high heating rates on the high-temperature oxidation and degradation of Cr-coated Zry-4 in steam above the eutectic temperature. Furthermore, it relates to a recent paper on the effect of Cr thickness on the oxidation and degradation of Cr-coated zirconium alloys [29]. That study showed that the optimum thickness of a PVD Cr-coating on Zircaloy-4 is in the range of 15–20 μm, which was also chosen for the present research.

2. Materials and methods

In this study, Zry-4 samples with and without Cr coatings were tested. The samples had the shape of a rod with 10.75 mm outer diameter and 9.3 mm inner diameter. The uncoated samples were 12 cm in length measured 12.5 cm with uncoated end plugs. The Cr coating, applied via physical vapor deposition (PVD) by Oerlikon Balzers Coating Germany GmbH, had a thickness of 15 μm. The rods were plugged, with the top plug featuring an M3 thread to simplify the attachment in the test facility. The initial microstructure is shown in Fig. 1 (the EBSD procedure is described below). The figure presents a 2D grain orientation map with the corresponding pole figures. The microstructure exhibits a columnar morphology of Cr grains, with finer grains located near the Zry-4 surface and progressively increasing grain size toward the outer layer. The plotted pole figures show formation of “cube” texture in the coating.

High-temperature oxidation tests were conducted using QUENCH-SR facility [30] at KIT. The aim was to investigate the impact of the heating rate on the oxidation of the rods in water vapor. The test run consisted of several steps that are described hereafter. A sample was heated up to 800 °C with a rate of 10 K/min in argon with the flow rate of 40 l/ h. Water vapour with a flow rate of 60 g/h was started, and the furnace was stabilized for 10 min at 800 °C. Then the transient oxidation step: heating to 1500 °C with various heating rates (5, 10, 30, 50, 100, and 300 K/min). After reaching 1500 °C, the power went off immediately, the steam was stopped and the specimens were cooled in the flowing argon gas. The heating profiles at various heating rates are schematically presented in Fig. 2, examples of set and measured temperatures with cooling profiles are shown in Appendix 1.

When interpreting the results, it is important to remember that the temperature was measured with some uncertainty originating from the facility design. First, inductive heating is less homogeneous than resistive heating, which can lead to variations in temperature depending on the position of the rod relative to the induction coil. Second, the inductor power was controlled by a pyrometer, while thermocouples were inserted into the sample only to record temperature. The pyrometer is more inert, and its measurements depend on the material’s reflectivity. As a result, while the pyrometer had not yet detected the maximum temperature, regions monitored by thermocouples may have already overheated. This caused temperature overshoot for samples heated at low heating rates and temperature undershoot for samples heated at high heating rates (examples of recorded parameters can be found in the Appendix 1). This phenomenon was also observed in our previous work with uncoated Zr-alloys [30], but with Cr-coated samples has become even more noticeable.

To evaluate the oxidation kinetics, we measured the H_2 release by an IPI GAM3000 mass spectrometer (InProcess Instruments GmbH, Bremen). The instrument was calibrated prior to testing, and the relative measurement uncertainty specified by the manufacturer is ±2%.

After all high-temperature oxidation tests, the samples were

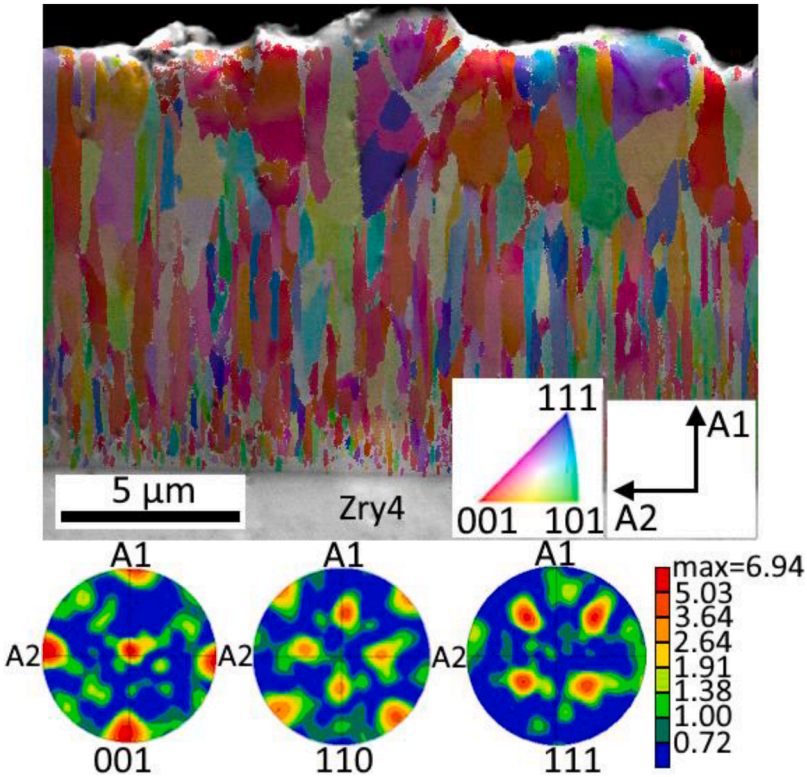

Fig. 1. EBSD analyses of as-coated samples.

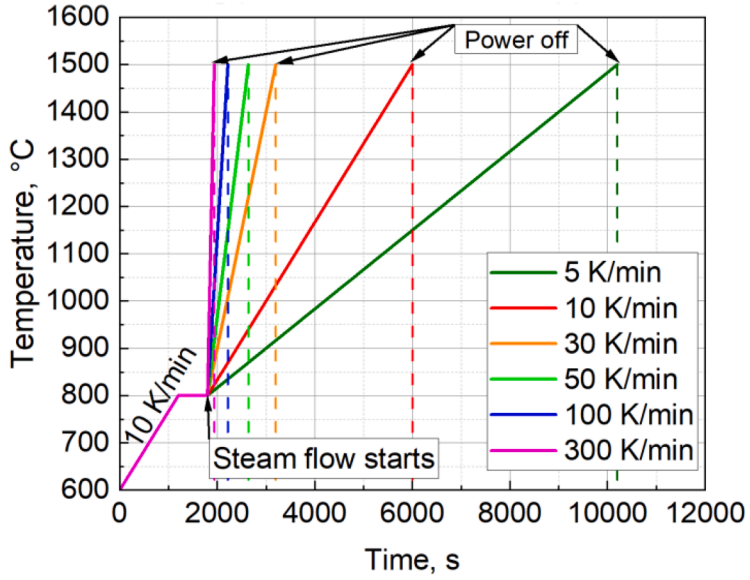

Fig. 2. Schematic diagram of the temperature program for all tests.

macroscopically and microscopically investigated. Macro images of specimens were taken with a digital camera (Canon EOS 1200D) at room temperature. The cross-sections of the middle parts of the rods were routinely prepared for optical and electron microscopy. Optical microscopy was done by inverted microscope Leica DMi8, electron microscopy was carried out by means of scanning electron microscopy (SEM) with energy dispersive spectroscopy (EDS, Philips XL 40S). Cross-sections of the samples were prepared by standard metallographic procedure and coated with a thin carbon layer for SEM imaging.

The Leica Microsystems DMi8 microscope allows the automatic creation of panoramic images of large cross-sectional areas. This capability enabled us to obtain images of the entire circle circumference of a rod. These images were also used to measure the area covered by the eutectic structure. Three cross sections were prepared from the middle part of each rod, closest to the thermocouple, with a spacing of 10 mm between adjacent sections. It was decided not to investigate cross

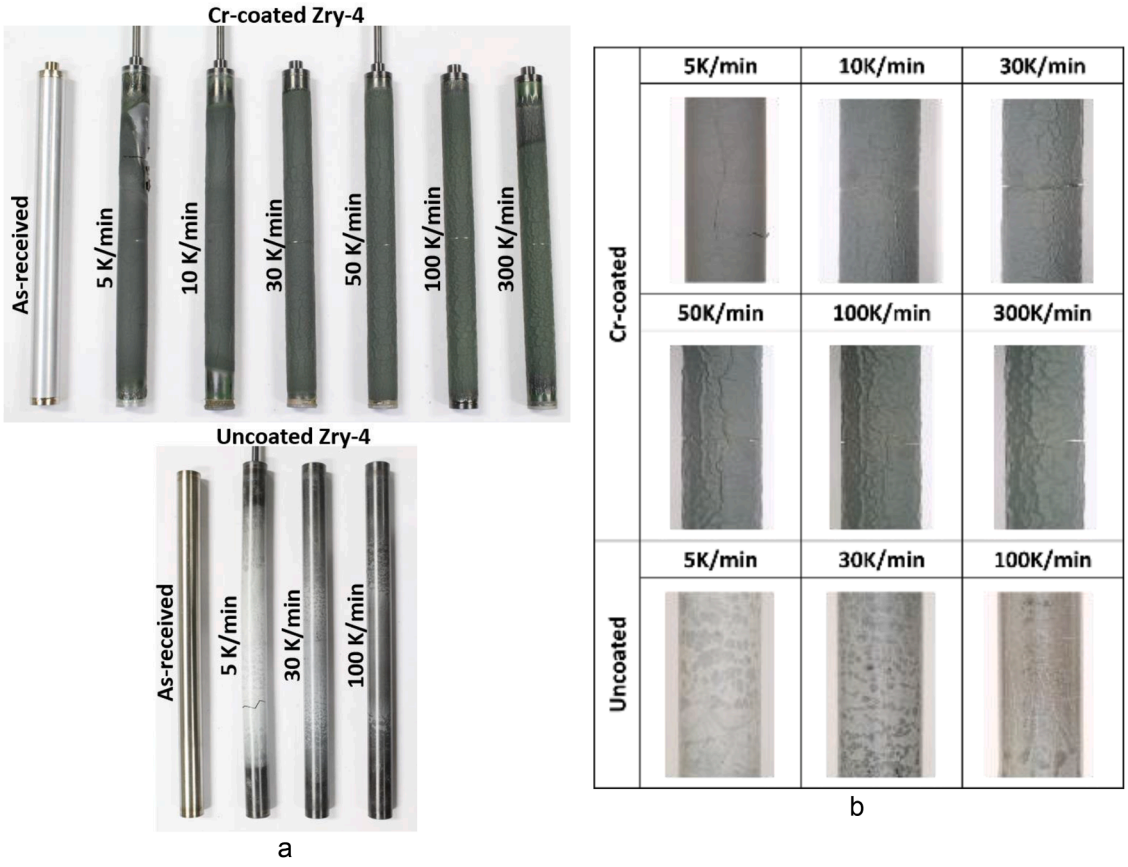

Fig. 3. Macro images of the rods after tests: **a.** overall view, **b.** midsections.

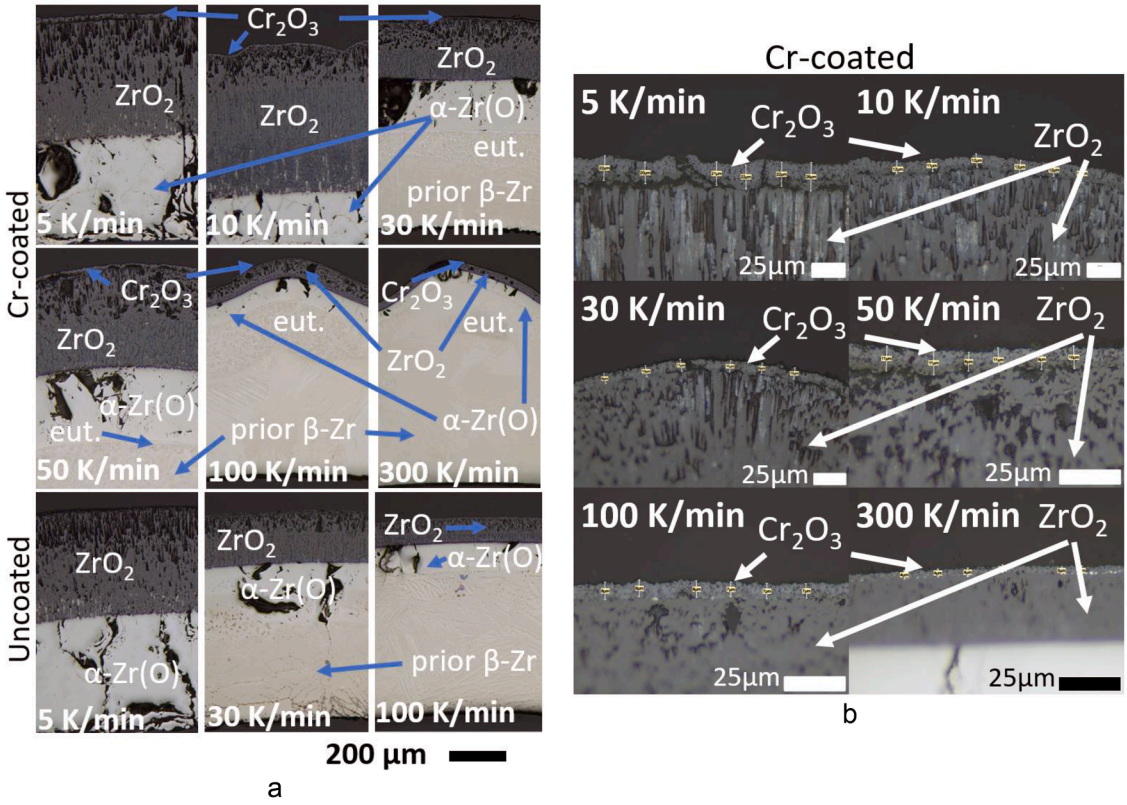

Fig. 4. OM images of cladding cross-sections: **a.** representative views showing the full cladding wall thickness, **b.** magnified images of the Cr_2O_3 layers in Cr-coated samples.

sections located far from the thermocouples due to the uncertainties mentioned above. Using the ImageJ software, the eutectic regions were manually outlined and their areas measured.

Electron Backscatter Diffraction (EBSD) was collected with a high-resolution field emission SEM MERLIN (Carl Zeiss Microscopy) equipped with a high-speed data collection EBSD system Hikari XP (EDAX Inc.). The samples for EBSD were embedded using a conductive mounting medium and prepared metallographically, with the final step consisting of vibratory polishing. For the sample tested at 300 K/min, the aim was to investigate the outer layer of the oxides. To ensure high polishing quality of this layer, a thin layer of Au was applied to the area of interest prior to embedding.

3. Results

3.1. Macro- and microscopic examinations

Fig. 3 shows macro images of the samples and magnified specimen midsection. After the tests, the uncoated Zry-4 exhibited white and grey surfaces. As the heating rate increased, the surface colour turned grey. Change of the oxide film colour from grey to white is the sign of the film degradation and loss of its adherence [31]. Cracks were only visible on the surface of the uncoated Zry-4 with 5 K/min. After testing, the Cr-coated samples exhibited a colour change ranging from grey to green, with greater green intensity observed at higher heating rates. The surface colour correlates with the Cr_2O_3 thickness: thinner oxides appear greener. Cracks were observed only on the sample with the slowest heating rate, i.e.5 K/min. The other samples exhibited the formation of the so-called "crocodile skin". Due to temperature overshooting, the upper part of the coated sample melted at 5 K/min.

Fig. 4 shows optical micrographs of the oxide layers and Fig. 5 presents their measured thicknesses. Only one representative position for each rod is shown in Fig. 4; panoramic views of the corresponding cross-sections are provided in Appendix 2. These images demonstrate that the oxide layer thickness may vary around the circumference of the cladding. This was especially noticeable for samples tested at 5 K/min, showing that both coated and uncoated claddings exhibit regions ranging from fully to partially oxidised across the cladding thickness. In the OM images (Fig. 4a), the dark grey regions correspond to oxide layers, whereas the lighter regions correspond to metallic Zr phases. Fragmented grains within the metallic phase indicate the presence of the brittle α-Zr(O) phase. With increasing heating rates, oxidation and the formation of α-Zr(O) were reduced. Fig. 4b shows locations containing Cr_2O_3 layer. The thickness of this oxide was uniformly distributed in the circumference.

Fig. 5 presents average oxide thickness with corresponding error bars. The oxide thicknesses were measured on a central cross-section along the entire circumference, using 10 to 60 measurement points, depending on how uniform the oxide thickness was. The thicknesses of both oxide layers decrease with increasing heating rate according to an inverse power law. The measured ZrO_2 data were also compared with calculated values for uncoated Zr-alloys using the Cathcart–Pawel and Urbanick–Heidrick models [32]. The calculations were performed assuming ZrO_2 growth within the temperature range of 1300–1500 °C. The measured values agree with the model predictions starting from heating rates of 30 K/min. At lower heating rates, the measured ZrO_2

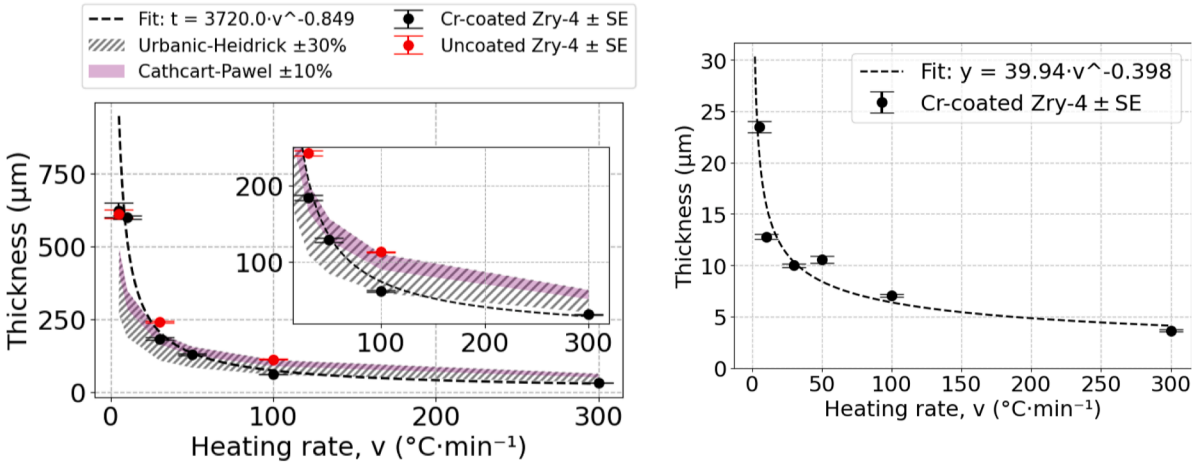

Fig. 5. Measured thickness of oxide layers.

thicknesses were larger, most likely due to temperature overshoot. The agreement is especially good with the Urbanick–Heidrick model, whose error bars cover a wider range. The measured ZrO_2 thicknesses of uncoated Zircaloy-4 were close to those of the coated samples, indicating similar oxidation kinetics.

The thickness of Cr_2O_3 also decreases with heating rate following an inverse power law, but it decreases less steeply than ZrO_2 and remains on the order of only several micrometres at 300 K/min.

SEM images obtained by BSE along with EDS maps are shown in Fig. 6. In Cr-coated Zry-4 specimens, the outermost Cr coating was fully transformed into Cr_2O_3 or consumed for eutectic formation. Beneath the Cr_2O_3 layer, a ZrO_2 layer was identified, followed by ZrO_2 containing α-Zr(O) precipitates formed during phase transformation from cubic $ZrO_{(2-x)}$ to tetragonal ZrO_2. Due to the brittleness of the α-Zr(O) phase, cracking was commonly observed in this layer. With increasing heating rate, the ZrO_2 and α-Zr(O) layers became thinner.

Although the "crocodile skin" was already observed on the surface of the 10 K/min sample, a distinct eutectic structure on the cross-section was first formed starting at 30 K/min. Prior-β-Zr also retained at 30 K/min. At lower heating rates (5 and 10 K/min), EDS analyses revealed that chromium diffused into α-Zr(O) in the direction of inner surface, forming a multiphase structure with Sn, that, however, lacked a typical eutectic morphology (red dashed area in Fig. 6).

At 50, 100 and 300 K/min, a similar phase structure was observed as at 30 K/min, including Cr_2O_3, ZrO_2, α-Zr(O), prior-eutectic, and prior-β-Zr. Eutectic covered a significant area, suggesting extensive Cr–Zr interaction. Areas covered by eutectic structure were measured on three cross-sections of each rod:

- 30 K/min: 2.6 ± 0.5 mm^2
- 50 K/min: 4.2 ± 1.4 mm^2
- 100 K/min: 4.2 ± 0.6 mm^2
- 300 K/min: 3.6 ± 0.3 mm^2

The measurements revealed no clear correlation between the eutectic area and the heating rate. However, with increasing heating rate, both the prior-β-Zr and dendritic lamellae became finer (Appendix 3). Interestingly, in the 30 K/min sample an additional globular crystalline phase with bright contrast was observed (Fig. 7 and Table 1). It appeared in the form of lamellae as well as large, non-uniform crystals (P2 and P7) and was not observed in other samples. The lamellar structure was especially noticeable near the α-Zr(O) (P6, P8). This phase consisted mainly Zr and O, along with several at% of Fe and Cr, indicating that Fe from the Zry-4 also participates in the eutectic process. In the interlamellar regions (P1, P4) Zr contains a higher chromium concentration than the α-Zr(O). However, the EDX results should be

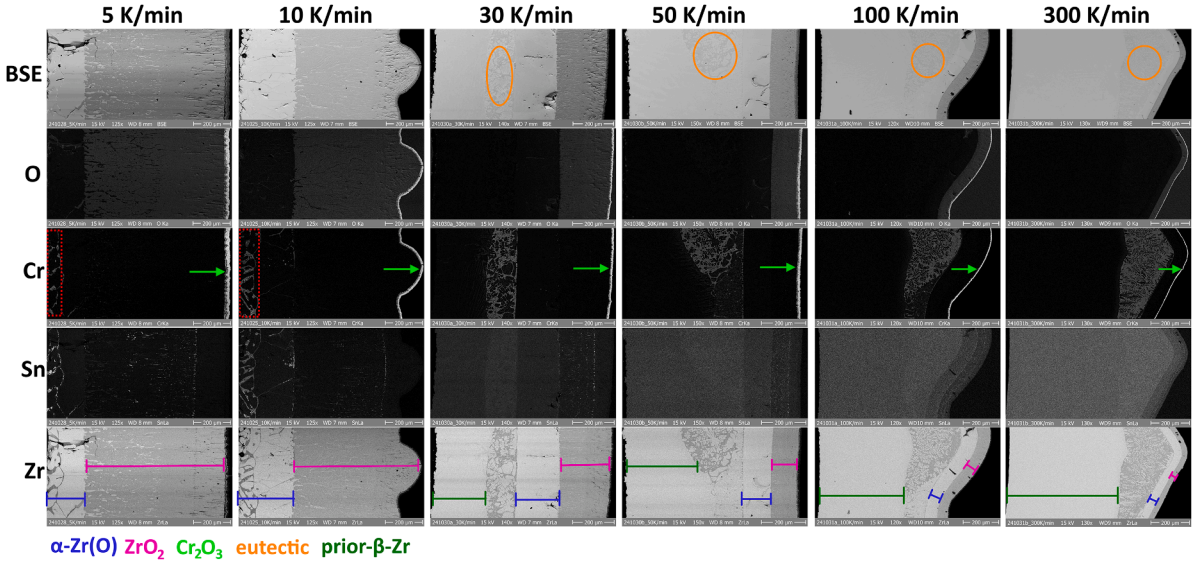

Fig. 6. SEM-BSE images with EDX maps of claddings midsections.

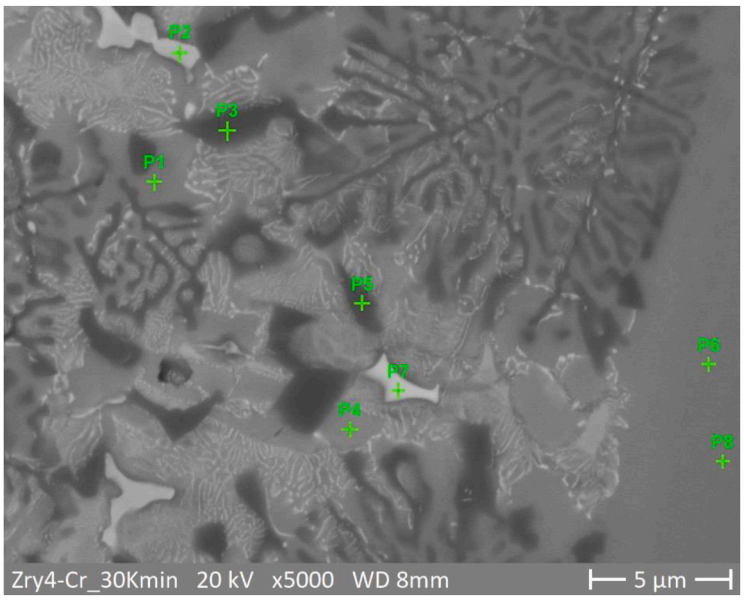

Fig. 7. Magnified image of the prior-eutectic structure in the sample tested at 30 K/min, showing the presence of a distinct bright-contrast phase.

Table 1
EDS analysis of the eutectic structure in the sample tested at 30 K/min (Fig. 7).

EDS Point	OKa A%	CrKa A%	FeKa A%	ZrLa A%	SnLa A%
P1	7.1	26.0	1.8	63.5	1.6
P2	7.5	3.9	8.0	79.8	0.9
P3	6.6	55.9	4.7	32.4	0.4
P4	6.1	1.4	1.3	89.0	2.3
P5	3.4	53.0	8.2	34.9	0.5
P6	10.2	1.1	1.3	86.5	0.8
P7	9.3	2.9	5.5	81.2	1.1
P8	13.8	0.8	1.1	83.0	1.2

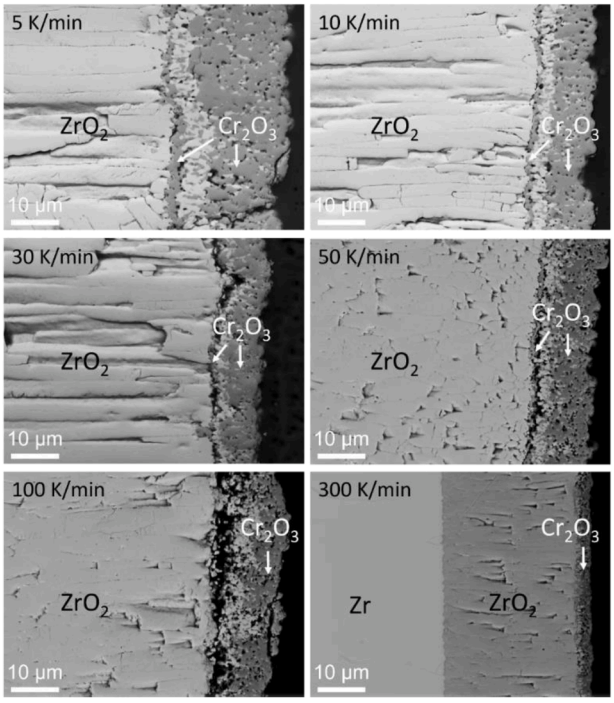

Fig. 8. SEM-BSE Images of the outer surface.

interpreted with caution, because the detected signal can be also collected from materiel beneath the analysed surface. The black phase on the image (P3 and P5) corresponds to $ZrCr_2$.

Fig. 8 shows magnified images of the Cr_2O_3 on the surface. The Cr_2O_3 layer appeared porous with numerous voids. The Cr_2O_3 layer typically contains an intermediate ZrO_2 layer positioned a few micrometres away from the interface, adjacent to the elongated ZrO_2 layer, thereby forming a thin Cr_2O_3 gap. With the raising heating rate this gap becomes less intact with the grains falling out.

We analysed these layers in more detail at the heating rate of 300 K/min and found that the transition from ZrO_2 to Cr_2O_3 differed from that observed at lower heating rates. At low heating rates, ZrO_2 typically forms a direct interface with Cr_2O_3. However, at 300 K/min between these two phases a pure Cr-layer was identified (Fig. 9). According to Brachet's model ($\Delta Cr_{(Cr2O3\ +\ Cr\ diffusion\ into\ \beta-Zr)} = 6730exp(15784/T) \times \sqrt{t}$) [33] we calculated that at 300 K/min only 2 µm of Cr should have been consumed before eutectic reaction, so the remaining Cr to react at 1330 °C was 13 µm. These 13 µm are expected to have been consumed

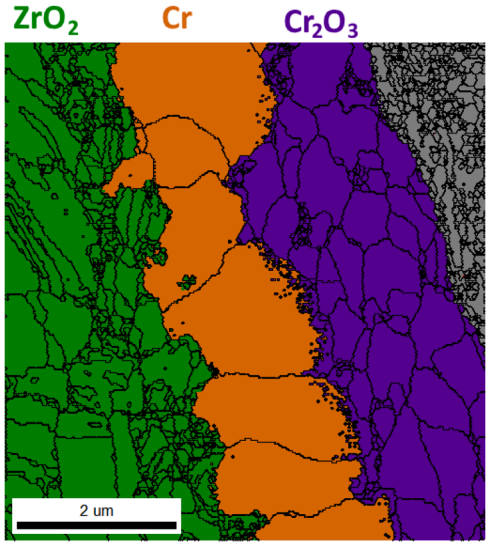

Fig. 9. EBSD Phase map of the outer surface of the oxide layers of the 300K/min sample.

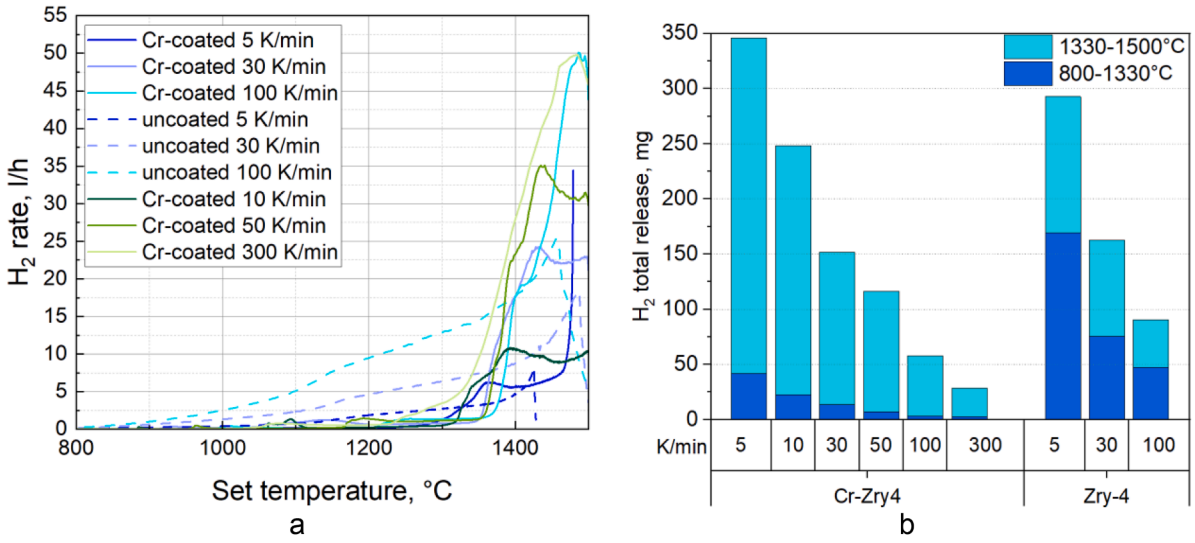

Fig. 10. a. H_2 release rate, **b.** Total H_2 release.

during the formation of the eutectic structure. Therefore, the layer shown in Fig. 7 is presumed to correspond to unreacted chromium. However, because Cr_2O_3 reduction occurs during the oxidation process, it cannot be ruled out that this layer is at least partially composed of chromium originating from the reduction of Cr_2O_3.In contrast, at lower heating rates, the phases are distinctly separated: elongated ZrO_2 followed by Cr_2O_3, within which a thick ZrO_2 layer and subsequent intergranular ZrO_2 were formed. This ZrO_2 is the product of Cr_2O_3 reduction, which occurs due to the higher affinity of Zr to oxygen [26].

3.2. H_2 release

During the tests, hydrogen release was measured using mass spectrometry. As the mass gain cannot be measured in situ in this type of experiment, the hydrogen release rate serves as an indicator of the oxidation rate [34]. Fig. 10 shows the H_2 release rate (Fig. 10a) and the total H_2 release during the test (Fig. 10b). In Fig. 10a, coated and uncoated samples are compared. It can be clearly seen that for the uncoated samples, the H_2 release gradually increased with temperature. In contrast, the coated samples exhibited relatively low H_2 release up to the eutectic temperature (≈1330 °C), after which the release sharply increased. Each curve, except for the one at 300 K/min, shows two maxima similar to the behaviour observed on sheet samples [15]. The first maximum shifts to higher temperatures with increasing heating rate, while the second appears at around 1500 °C. The second maximum is particularly pronounced in the 5 K/min sample; however it is due to the melting of the sample and starting of the oxidation of uncoated inner surface [23]. The curve for the 300 K/min sample exhibits only one maximum. It could be expected that this maximum would shift to even higher temperatures and that a second maximum might appear if the test were continued further. The reason for that is discussed in Section 4.3.

The total H_2 release decreased with the heating rate (Fig. 10b). The maximum amount of H_2 released during the oxidation of Cr-coated samples was observed at a heating rate of 5 K/min, while the minimum, approximately eight times lower, was recorded at 300 K/min. The values reported for 5 K/min include all hydrogen released from both the external and internal surfaces of the rod following melting. At lower heating rates, the longer oxidation time contributes to the higher total H_2 release. However, the main contribution to H_2 release occurred after the eutectic reaction.

In Fig. 10b, dark blue bars represent the total release in the range of 800–1330 °C, while light blue bars correspond to the release in the range of 1330–1500 °C. The fraction of H_2 released above 1330 °C accounted for 87.89% (5 K/min), 88.53% (10 K/min), 85.82% (30 K/min), 86.01% (50 K/min), 77.83% (100 K/min), and 61.7% (300 K/min) of the total release, respectively. In contrast, hydrogen release from uncoated samples was approximately equally distributed between these two temperature ranges.

The total amount of H_2 released from coated samples was higher only at 5 K/min. At heating rates of 30 K/min and especially 100 K/min, the total hydrogen release was noticeably lower than that observed for uncoated claddings.

4. Discussion

4.1. Comparison with experiments in oxygen

The current research is complementary to our previous research carried out by TGA device in oxygen atmosphere at 5, 10, 30, 50 K/min [9].

Macroscopically, a *crocodile-skin* pattern was observed starting from 10 K/min in both studies, and its coarseness increased with heating rate. However, at 50 K/min in oxygen, the surface exhibited a metallic colour with green islands, whereas in steam the surface was entirely green. The green coloration corresponds to Cr_2O_3. This difference can be attributed to the oxide uniformity: in the oxygen experiment, the Cr_2O_3 layer was thin and non-uniform and was not seen in some areas, while in steam it was thin but uniformly distributed across the investigated region. In both experiments, the Cr_2O_3 scale remained porous, which is believed to result from its reduction by the available Zr [26] and possibly by $Zr(Cr, Fe)_2$ [35], whereas volatilisation of chromium-containing species is expected to be negligible [36].

The oxide thickness varied significantly between the two experiments: ZrO_2 was noticeably thicker in steam experiments at comparable heating rates. In oxygen, the thickness of the zirconium oxide remained almost constant, whereas in steam it gradually decreased from approximately 600 μm at 5 K/min to about 100 μm at 50 K/min. In oxygen, a ZrO_2 layer approaching 200 μm was observed only at 2 K/min. However

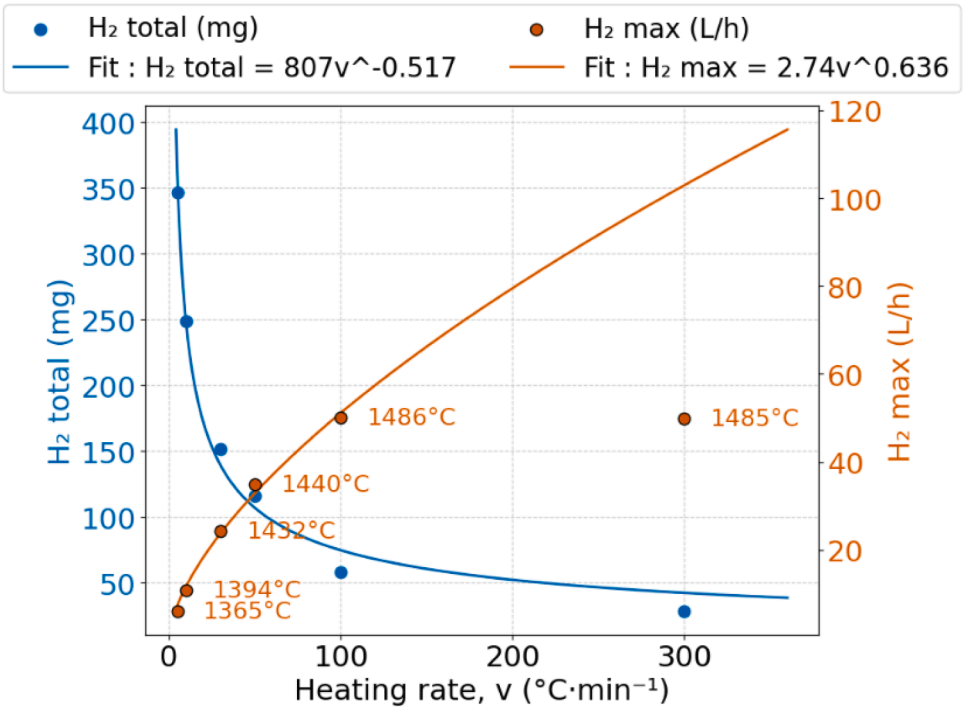

Fig. 11. Effect of heating rates on hydrogen release parameters.

as pointed out above, samples at 5 at 10 K/min experienced a significant temperature overshoot.

The eutectic reaction was also more pronounced in the oxygen experiments than in steam. In oxygen, eutectic formation was already observed at 5 K/min, whereas in steam it appeared only at 30 K/min. This may be due to intensified oxidation in steam and the earlier formation of α-Zr(O).

4.2. *Effect of high heating rates on the microstructure*

It is well known that a Cr coating fails once the eutectic temperature is exceeded. At this point Cr_2O_3 fails due to redox reaction, exposing Zr from the eutectic structure to steam [23]. In the present experiment, the extent of oxidation strongly depends on the heating rate, since higher heating rates result in shorter exposure times to the oxidising environment. Below 30 K/min, continuous diffusion leads to the growth of a thick ZrO_2 layer, whereas at higher rates, ZrO_2 formation is reduced due to the limited reaction time. At 300 K/min, representative of accidental conditions, ZrO_2 thickness is reduced to only a few tens of micrometres.

Only after 300 K/min was a pure Cr-coating identified, hence it was mostly consumed for oxidation and eutectic formation. Cr_2O_3 formed at all heating rates. Its thickness decreased with increasing heating rate and reached several tens of micrometres at 5 K/min, but was limited to only a few micrometres at 300 K/min.

Significant eutectic microstructure in the bulk Zircaloy was observed at heating rates of 30 – 300 K/min while at lower heating rates (5 and 10 K/min) a multiphase layer containing Cr and Sn only formed at the inner surface of the rods. We consider that this formed due to Cr diffusion [22] and local Sn enrichment. With increasing time, the diffusion of Cr in β-Zr towards Cr-free areas is enhanced[17]. Simultaneously, oxygen uptake promotes β → α transformation, but α-Zr dissolves significantly less Cr than β-Zr. The ongoing transformation progressively reduces the volume fraction of β-Zr and drives the β/α interface inwards until no β-Zr remains, thereby expelling Cr from the α-Zr grains. Sn also has a lower solubility in α-Zr than in β-Zr, and this solubility decreases further upon cooling, resulting in the formation of an Sn-enriched phase.

Only in the sample heated at 30 K/min did a phase with bright contrast, appearing as lamellae and non-uniform crystals, form. A similar globular α-phase has previously been reported in the pseudo-binary Zircaloy–O diagram [37] and is typical of oxygen-containing Zircaloy. We suppose that the longer oxygen exposure at this heating rate, compared with the faster-heated samples, promoted a thermodynamic equilibrium to form a ternary mechanical mixture of Zr–Cr–O. Based on previous tests, it was expected that higher heating rates would promote more eutectic microstructure, since more Cr should remain available to interact with Zr upon reaching the eutectic temperature. However, our results showed no correlation between the eutectic area and the heating rate. This may be due to two competitive phenomena: although at higher heating rates more Cr should remain to interact with the Zr-substrate, the limited time limits the formation of eutectic, because eutectic reaction needs time to develop [38].

4.3. *Effect of high heating rates on the H_2 release*

We analysed the total H_2 production and the maximum H_2 release rate (Fig. 11), which can be used as a measure of the oxidation rate, since H_2 is a product of the oxidation reaction. The fit to the data for the maximum release rate was performed only up to a heating rate of 100 K/min, because we assume that the maximum corresponding to 300 K/min was not reached.

As expected, hydrogen release from Cr-coated samples is suppressed until the eutectic temperature (T_e) is reached. After reaching T_e, the H_2 release increases sharply (Fig. 10a), and the maximum release rate increases approximately proportionally to the square of the heating rate (Fig. 11a). These maximum release rates also shift to higher temperatures, which may be attributed to the onset of the Zr–Cr eutectic reaction

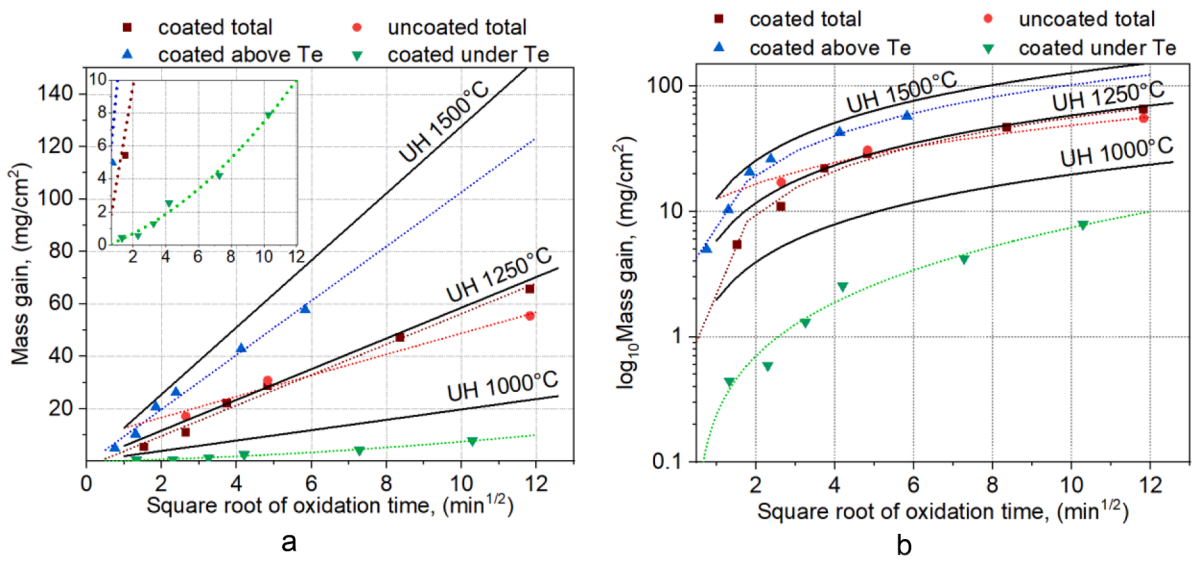

Fig. 12. Mass gain calculated from hydrogen release data as a function of the square root of oxidation time: **a.** linear scale, **b.** semi-log scale.

occurring at higher temperatures. In contrast to oxidation in oxygen [9], where this acceleration was observed in the mass gain, it is not straightforward to determine from the present results whether the slope of the hydrogen release curve becomes steeper with increasing heating rate. Nevertheless, it is evident that the slopes at lower heating rates are less steep, whereas those at 30, 50, and 100 K/min are relatively similar. In contrast, the curve obtained at 300 K/min exhibits a more gradual increase.

The appearance of several release peaks (Fig. 10a) corresponds to crystallographic phase transitions of ZrO_2, which have also been reported for various Zr alloys [39]. In the present case, the second peak is associated with the tetragonal-to-cubic ZrO_2 transition. This behaviour has previously been observed for Cr-coated samples and was reported for plate samples heated at 10 K/min [15].

It is particularly interesting to compare these results with the performance of cold-sprayed coating under similar conditions [16]. The maximum H_2 release of the cold-sprayed sample at 10 K/min was around 7 l/h at 1450 °C, whereas the PVD-coated sample investigated in the present study reached a peak value of approximately 10 l/h. Unlike the PVD-coated sample, the cold-sprayed sample did not exhibit two distinct oxidation peaks. Instead, oxidation accelerated at approximately 1250 °C, followed by a sharp increase in hydrogen release at around 1420 °C. During the initial oxidation acceleration, a small peak was observed near the eutectic temperature; however, this peak was significantly lower than the one observed at 1450 °C, reaching only about 2 l/h.

The total H_2 release decreases with the inverse square root of the heating rate. Although the H_2 release at temperature above T_e increases dramatically, the total amount of H_2 produced at high heating rates is lower than that observed for uncoated Zry-4 cladding tubes. However, under real accident conditions, the fuel rods will continue to be heated internally, which may lead to prolonged H_2 production.

Nevertheless, it is important to determine whether the observed trends are a genuine effect of the heating rate or simply a consequence of the oxidation time. To investigate this, the mass gain calculated from hydrogen release was evaluated as a function of time, as shown in Fig. 12. This calculation is based on the oxidation reaction of zirconium in steam and the molar masses of the reaction products, yielding a mass gain-to-hydrogen release ratio of 8:1. For the total mass gain, the shown time corresponds to the heating period from 800 to 1500 °C, for oxidation below the T_e – 800–1330 °C, whereas for oxidation above T_e – 1330–1500 °C. In addition, theoretical mass gains were calculated using the Urbanic–Heidrick (UH) correlation for isothermal oxidation at 1000 °C, 1250 °C, and 1500 °C.

Fig. 12a shows that the experimental data exhibit pure parabolic behavior for the total mass gain, the mass gain above T_e, and the uncoated sample. In contrast, the data corresponding to oxidation below T_e (i.e., oxidation of Cr and oxygen diffusion into the substrate) deviate from a purely parabolic trend, that was also described in [34].

In semi-log scale (Fig. 12b), the characteristics of the mass gain curves can be compared more easily. Overall, the theoretical and experimental curves exhibit similar behaviour. As expected, the data obtained for oxidation in the range of 1330–1500 °C lie below the UH curve at 1500 °C, because the material experienced oxidation at lower temperatures before reaching 1500 °C. Interestingly, the total mass gain for both coated and uncoated samples matches the theoretical values at 1250 °C, which is close to the midpoint of the investigated temperature range from 800 °C to 1500 °C (i.e. 1150 °C). These observations suggest that the measured oxidation behavior is primarily governed by oxidation time with no clear evidence of an additional heating-rate effect.

Although the microstructural differences and mass gains observed at different heating rates can largely be attributed to variations in oxidation time, the peak hydrogen release rate is directly influenced by the heating rate itself. In the present study, it is clearly seen that the maximum hydrogen release rate increases with increasing heating rate (brown curve in Fig. 11). It means that the heat generation rate grows as well. These observations support previously reported behaviour [9] and confirm that the resulting temperature escalation may exceed the heat produced by fission decay, thereby contributing to further temperature escalation.

5. Conclusions

The effect of the heating rate on the oxidation behaviour of Cr-coated

Zry-4 was investigated in this work using the QUENCH-SR facility in steam up to 1500 °C, at heating rates of 5, 10, 30, 50, 100, and 300 K/min.

Microstructural investigations revealed the formation of a *crocodile-skin* morphology at heating rates ≥ 10 K/min/; however, a clearly developed eutectic microstructure was first observed at

30 K/min. At lower heating rates, the samples fully oxidized. At heating rates ≥ 30 K/min, eutectic structures formed. With increasing heating rate (and thus decreasing exposure time), the eutectic structure became finer; however, no clear correlation between the eutectic area fraction and the heating rate was observed. The thicknesses of both ZrO_2 and Cr_2O_3 oxide layers decreased with increasing heating rate, following an inverse power-law, with the Cr_2O_3 layer decreasing more slowly.

Hydrogen release measurements revealed that oxidation of Cr-coated tubes occurs predominantly above the eutectic temperature and is characterized by accelerated oxidation. The peak oxidation rates increase approximately with the square root of the heating rate and shift to higher temperatures as the heating rate increases. Nevertheless, the total hydrogen release (i.e., the overall extent of oxidation) decreases with increasing heating rate, following an approximate inverse square-root trend. Already at a heating rate of 30 K/min, Cr-coated tubes released less hydrogen than uncoated Zry-4 tubes.

The main outcomes of this work are as follows:

- although the Cr coating exhibits accelerated oxidation after the eutectic reaction compared to uncoated samples, it leads to reduced total hydrogen production at the higher heating rates relevant to severe accident conditions,
- effect of heating rate on the oxidation behaviour is largely attributable to its influence on exposure time. The main exception is the peak heat release rate, which increases with increasing heating rate.

Declaration of generative AI use

The authors used Chat GPT (OpenAI) to assist with English language editing and grammar correction. All scientific content was produced by authors.

CRediT authorship contribution statement

Diana Bachurina: Writing – original draft, Investigation, Formal analysis. **Jaeyoon Bae:** Visualization, Investigation, Formal analysis. **Ulrike Stegmeier:** Writing – review & editing, Methodology, Investigation. **Martin Steinbrueck:** Writing – review & editing, Funding acquisition, Conceptualization.

Declaration of competing interest

The authors declare that they have no known competing financial interests or personal relationships that could have appeared to influence the work reported in this paper.

Acknowledgements

The authors acknowledge the Korea Nuclear International Cooperation Foundation (KONICOF) for supporting a six-month internship at the Karlsruhe Institute of Technology (KIT) for one of the authors.

Appendix 1

Recorded experimental parameters for samples heated at 5 K/min and 300 K/min illustrating transient temperature over- and undershooting

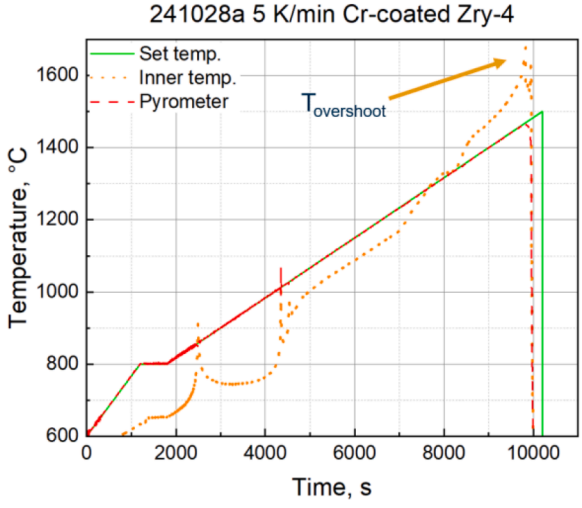

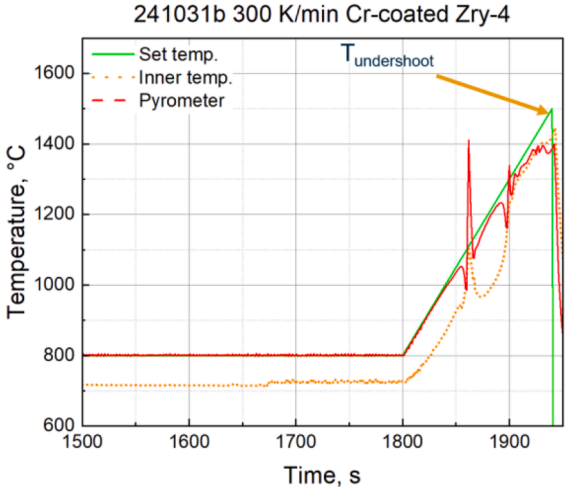

Appendix 2

Magnified images of oxide layers of the rods. On the lefthandside one can see that the dark grey area corresponds to oxide layers both ZrO2 and Cr2O3. These are representative pictures of oxide layers where metaalic Zr-phase remains. On the right handside one can se e representative images of measured Cr2O3 layers.

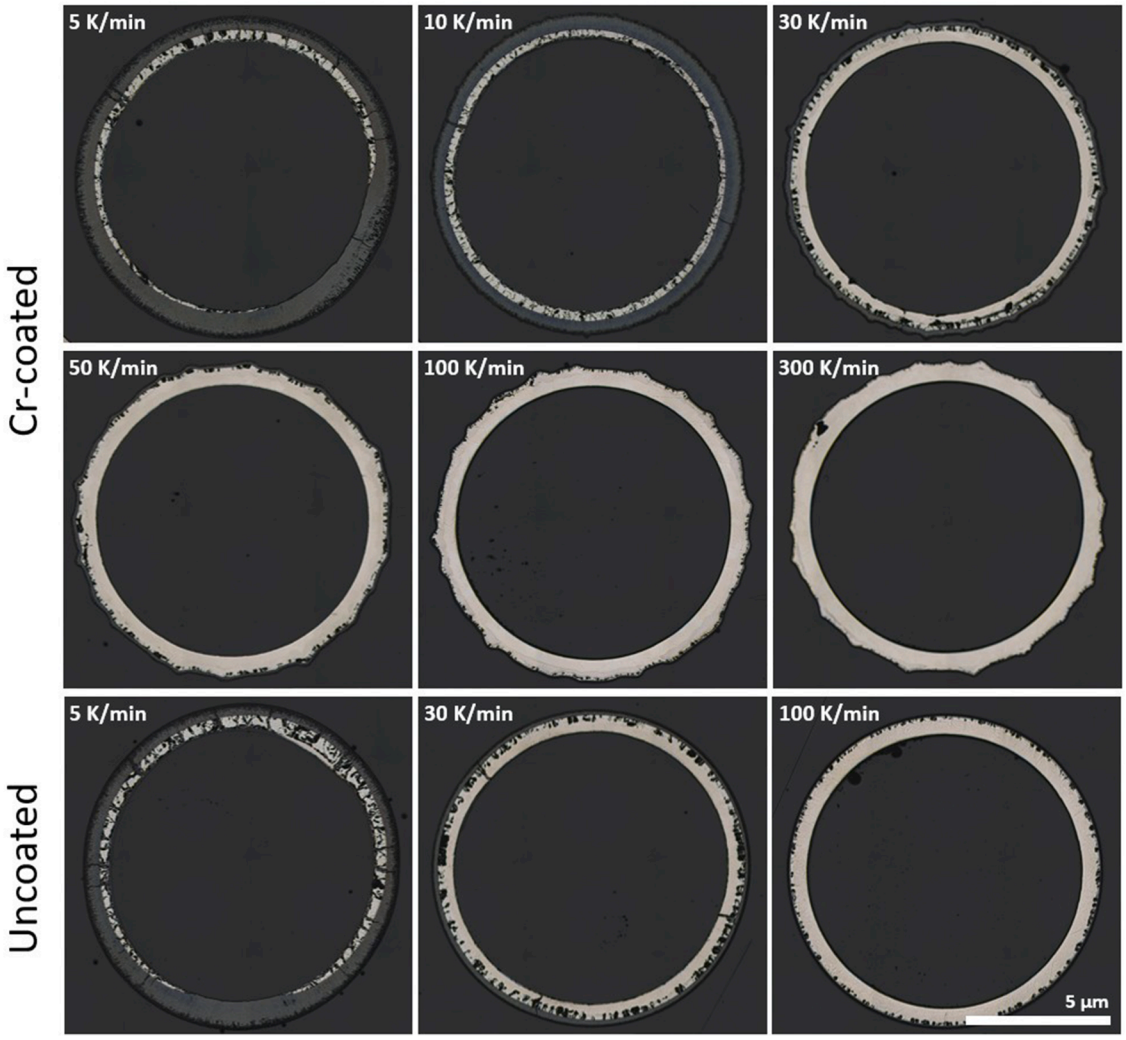
Cr-coated
Uncoated
5 K/min
10 K/min
30 K/min
50 K/min
100 K/min
300 K/min
5 K/min
30 K/min
100 K/min
5 µm

Appendix 3

Magnified images of Zr-Cr eutectic microstructure formed at different heating rates. With the increasing heating rate prior-β-Zr dendrites become smaller as well as lamellas of the prior-eutectic phase.

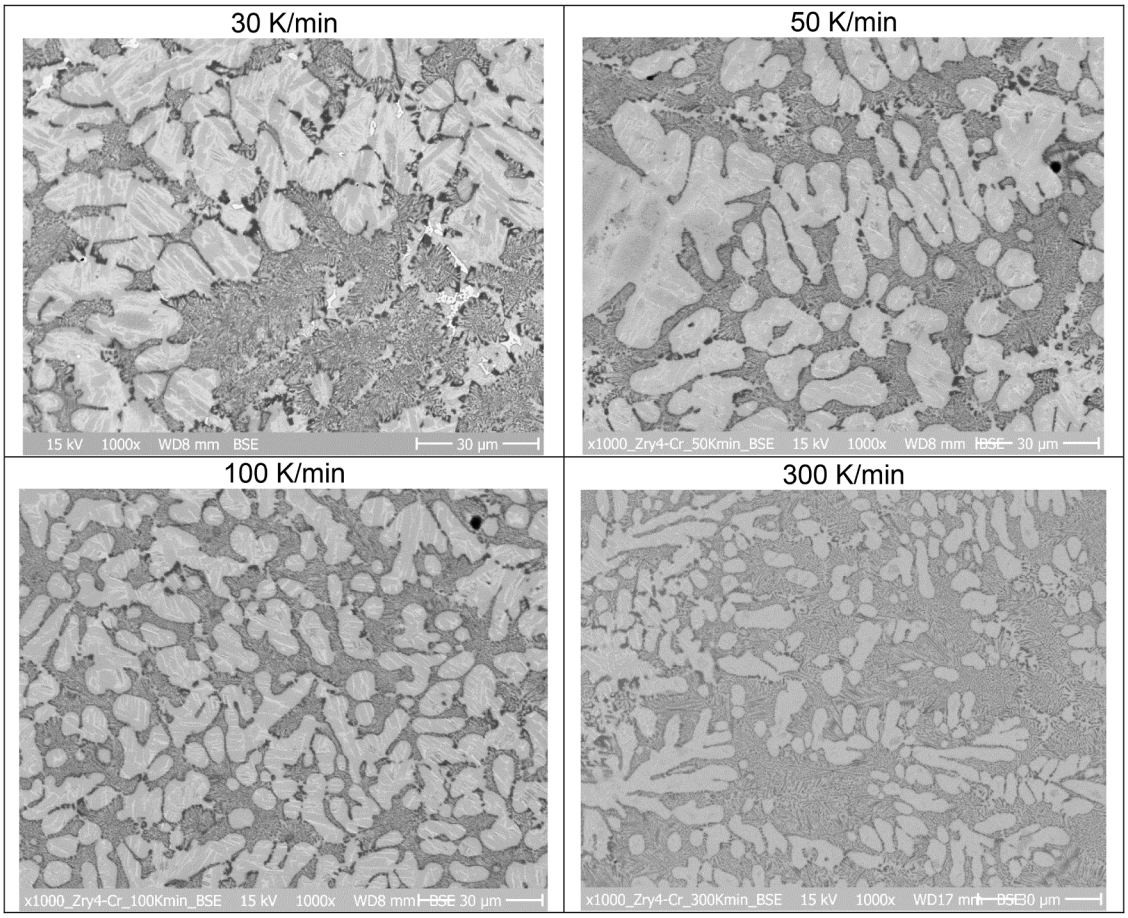

Data availability

Data will be made available on request.

References

[1] M. Steinbrueck, M. Grosse, C. Tang, J. Stuckert, H.J. Seifert, An overview of mechanisms of the degradation of promising ATF cladding materials during oxidation at high temperatures, High Temp. Corros. Mater. 101 (2024) 621–647, https://doi.org/10.1007/s11085-024-10229-y.

[2] J. Yang, M. Steinbrück, C. Tang, M. Große, J. Liu, J. Zhang, D. Yun, S. Wang, Review on chromium coated zirconium alloy accident tolerant fuel cladding, J. Alloys Compd. 895 (2022), https://doi.org/10.1016/j.jallcom.2021.162450.

[3] Y. Li, B.Q. Wang, X.Y. Zhang, S.J. Wang, C.Y. Li, H.L. Yang, R.R. Su, T. Liu, High-temperature oxidation behavior and degradation mechanism of chromium-coated zirconium alloy cladding: a review, Tungsten 7 (2024) 50–70, https://doi.org/10.1007/S42864-024-00289-7.

[4] C. Tang, M. Stueber, H.J. Seifert, M. Steinbrueck, Protective coatings on zirconium-based alloys as accident-Tolerant fuel (ATF) claddings, Corros. Rev. 35 (2017) 141–165, https://doi.org/10.1515/corrrev-2017-0010.

[5] K. Sakamoto, Y. Miura, S. Ukai, N.H. Oono, A. Kimura, A. Yamaji, K. Kusagaya, S. Takano, T. Kondo, T. Ikegawa, I. Ioka, S. Yamashita, Development of accident tolerant FeCrAl-ODS fuel cladding for BWRs in Japan, J. Nucl. Mater. 557 (2021) 153276, https://doi.org/10.1016/J.JNUCMAT.2021.153276.

[6] K.G. Field, Y. Yamamoto, B.A. Pint, M.N. Gussev, K.A. Terrani, Accident tolerant fecral fuel cladding: current status towards commercialization, Miner. Metals Mater. Ser. (2019) 1381–1389, https://doi.org/10.1007/978-3-030-04639-2_91/FIGURES/2.

[7] S. Suyama, M. Ukai, M. Uchihashi, H. Heki, S. Tajima, K. Okonogi, K. Kakiuchi, Development of accident tolerant SIC/SIC composite for nuclear reactor channel box, (2015) 35–42. https://doi.org/10.1002/9781119211709.CH4.

[8] H.V. Pham, M. Kurata, M. Steinbrueck, Steam oxidation of silicon carbide at high temperatures for the application as accident tolerant fuel cladding, an overview, Thermo 1 (2021) 151–167, https://doi.org/10.3390/THERMO1020011.

[9] D. Kim, M. Steinbrück, M. Grosse, C. Tang, Y. Lee, Eutectic reaction and oxidation behavior of Cr-coated Zircaloy-4 accident-tolerant fuel cladding under various heating rates, J. Nucl. Mater. 583 (2023) 154538, https://doi.org/10.1016/J.JNUCMAT.2023.154538.

[10] D. Wang, R. Zhong, X. Wu, Y. Zhang, X. Li, J. Yu, Y. Lan, G.H. Su, S. Qiu, W. Tian, Y. Liao, Z. Peng, C. Guo, Z. Song, J. Sun, Study on eutectic-oxidation coupling reaction of Cr-Zr system in high temperature steam environment, J. Nucl. Mater. 596 (2024) 155082, https://doi.org/10.1016/J.JNUCMAT.2024.155082.

[11] S. Wang, B. Yao, W. Zhai, Z. Li, J. Jiang, X. Ma, Evolution of the Zr-Cr eutectic structure and its effect on the oxidation mechanism of Cr-coated Zr alloy at 1350°C, Surf. Interfaces 62 (2025) 106221, https://doi.org/10.1016/J.SURFIN.2025.106221.

[12] J. Liu, C. Tang, M. Steinbrück, J. Yang, U. Stegmaier, M. Große, D. Yun, H. J. Seifert, Transient experiments on oxidation and degradation of Cr-coated Zircaloy in steam up to 1600 °C, Corros. Sci. 192 (2021) 109805, https://doi.org/10.1016/j.corsci.2021.109805.

[13] B. Kweon, H. Yook, D. Kim, Y. Lee, Assessment of the impact of Zr-Cr eutectic reaction on the structural integrity of Cr-coated ATF cladding, J. Nucl. Mater. 617 (2025) 156166, https://doi.org/10.1016/J.JNUCMAT.2025.156166.

[14] J.C. Brachet, E. Rouesne, J. Ribis, T. Guilbert, S. Urvoy, G. Nony, C. Toffolon-Masclet, M.L. Saux, N. Chaabane, H. Palancher, A. David, J. Bischoff, J. Augereau, E. Pouillier, High temperature steam oxidation of chromium-coated zirconium-based alloys: kinetics and process, Corros. Sci. 167 (2020), https://doi.org/10.1016/j.corsci.2020.108537.

[15] J. Liu, C. Tang, M. Steinbrück, J. Yang, U. Stegmaier, M. Große, D. Yun, H. J. Seifert, Transient experiments on oxidation and degradation of Cr-coated Zircaloy in steam up to 1600 °C, Corros. Sci. 192 (2021) 109805, https://doi.org/10.1016/J.CORSCI.2021.109805.
[16] C. Tang, M. Grosse, M. Steinbrueck, K. Shirvan, Oxidation and quench behavior of cold spraying Cr coated zircaloy fuel cladding under severe accident scenarios. TopFuel, 2019, p. 2019. Seattle, WA, USA.
[17] S.H. Joung, H. Yook, D. Kim, Y. Lee, Exploring the peak cladding temperature limit of Cr-coated ATf cladding by assessing the impact of the Zr-Cr eutectic on the structural integrity of cladding, J. Nucl. Mater. 605 (2025) 155577, https://doi.org/10.1016/J.JNUCMAT.2024.155577.
[18] E.B. Kashkarov, D.V. Sidelev, N.S. Pushilina, J. Yang, C. Tang, M. Steinbrueck, Influence of coating parameters on oxidation behavior of Cr-coated zirconium alloy for accident tolerant fuel claddings, Corros. Sci. 203 (2022) 110359, https://doi.org/10.1016/J.CORSCI.2022.110359.
[19] H. Liao, W. Huang, H. Ruan, T. Zhang, Y. Ning, P. Zhu, X. Xu, M. Xu, S. Yin, Y. Su, J. Wang, Oxidation behavior and microstructural evolution of Cr coatings prepared by multi-arc ion plating on Zry-4 in steam environments up to 1400°C, J. Nucl. Mater. 583 (2023) 154530, https://doi.org/10.1016/J.JNUCMAT.2023.154530.
[20] D. Wang, R. Zhong, Y. Zhang, P. Chen, J. Yu, Y. Lan, G.H. Su, S. Qiu, W. Tian, Y. Liao, Z. Peng, Oxidation behavior and kinetics of magnetron-sputtered Cr-coated Zr alloy cladding in 1000–1300 °C steam environment, Corros. Sci. 218 (2023) 111215, https://doi.org/10.1016/J.CORSCI.2023.111215.
[21] Y. Wang, Y. Wang, S. Wang, J. Geng, C. Zhang, Y. Zhao, W. Zeng, Systematic investigations on the oxidation mechanism of Cr coated Zr-4 alloy under different high-temperature steam conditions, Ceram. Int. 50 (2024) 17086–17096, https://doi.org/10.1016/J.CERAMINT.2024.02.185.
[22] J. Liu, M. Steinbrück, M. Große, U. Stegmaier, C. Tang, D. Yun, J. Yang, Y. Cui, H. J. Seifert, Systematic investigations on the coating degradation mechanism during the steam oxidation of Cr-coated Zry-4 at 1200°C, Corros. Sci. 202 (2022) 110310, https://doi.org/10.1016/J.CORSCI.2022.110310.
[23] D. Wang, R. Zhong, X. Wu, Y. Zhang, X. Li, J. Yu, Y. Lan, G.H. Su, S. Qiu, W. Tian, Y. Liao, Z. Peng, C. Guo, Z. Song, J. Sun, Study on eutectic-oxidation coupling reaction of Cr-Zr system in high temperature steam environment, J. Nucl. Mater. 596 (2024) 155082, https://doi.org/10.1016/J.JNUCMAT.2024.155082.
[24] S. Wu, X. Wu, Y. Zhang, D. Wang, P. Ma, W. Tian, S. Qiu, G.H. Su, Study on eutectic melting and high-temperature oxidation characteristics of Cr coated Zr alloy cladding under steam atmosphere at 1400–1500 °C, J. Alloys Compd. 1039 (2025) 183389, https://doi.org/10.1016/J.JALLCOM.2025.183389.
[25] S. Wang, B. Yao, W. Zhai, Z. Li, J. Jiang, X. Ma, Evolution of the Zr-Cr eutectic structure and its effect on the oxidation mechanism of Cr-coated Zr alloy at 1350°C, Surf. Interfaces 62 (2025) 106221, https://doi.org/10.1016/J.SURFIN.2025.106221.
[26] D. Kim, Y. Lee, Mechanisms of steam oxidation-induced degradation of chromium coating on zirconium alloys at high temperatures, Corros. Sci. 254 (2025) 113055, https://doi.org/10.1016/J.CORSCI.2025.113055.
[27] H. Yeom, B. Maier, G. Johnson, T. Dabney, M. Lenling, K. Sridharan, High temperature oxidation and microstructural evolution of cold spray chromium coatings on Zircaloy-4 in steam environments, J. Nucl. Mater. 526 (2019) 151737, https://doi.org/10.1016/J.JNUCMAT.2019.151737.
[28] E.B. Kashkarov, D.V. Sidelev, M.S. Syrtanov, C. Tang, M. Steinbrück, Oxidation kinetics of Cr-coated zirconium alloy: effect of coating thickness and microstructure, Corros. Sci. 175 (2020) 108883, https://doi.org/10.1016/J.CORSCI.2020.108883.
[29] M. Steinbrueck, I. Lee, U. Stegmaier, C. Tang, M. Stueber, Oxidation and degradation of Cr-coated Zr-based alloy up to 1500°C: effect of Cr thickness, J. Nucl. Mater. 625 (2026) 156520, https://doi.org/10.1016/j.jnucmat.2026.156520.
[30] M. Steinbrück, U. Stegmaier, M. Große, L. Czerniak, E. Lahoda, R. Daum, K. Yueh, High-temperature oxidation and quenching of chromium-coated zirconium alloy ATF cladding tubes with and w/o pre-damage, J. Nucl. Mater. 559 (2022) 153470, https://doi.org/10.1016/J.JNUCMAT.2021.153470.
[31] T. Alam, M.K. Khan, M. Pathak, K. Ravi, R. Singh, S.K. Gupta, A review on the clad failure studies, Nucl. Eng. Des. 241 (2011) 3658–3677, https://doi.org/10.1016/J.NUCENGDES.2011.08.009.
[32] G. Schanz, B. Adroguer, A. Volchek, Advanced treatment of zircaloy cladding high-temperature oxidation in severe accident code calculations Part I. Experimental database and basic modeling, Nucl. Eng. Des. 232 (2004) 75–84, https://doi.org/10.1016/j.nucengdes.2004.02.013.
[33] J.-C. Brachet, T. Guilbert, D. Hamon, G. Nony, P. Gokelaere, A new « ECR » parameter to support high-temperature (one-sided) steam oxidation behavior of Cr-COATED Zr-BASED E-ATF claddings, in relation with their post-quenching (PQ) mechanical strength and ductility (for loca and slightly beyond conditions), in: Topfuel /Reactor Fuel Performance" International Symposium, Grenoble, France, 2024.
[34] J.C. Brachet, T. Guilbert, S. Urvoy, E. Rouesne, M. Peyret, T. Vandenberghe, C. Prou, T.L. Hong, D. Hamon, Some practical methodologies to assess the overall high temperature (one-sided) steam oxidation protectiveness of chromium-based coatings on a zirconium-based substrate, as enhanced – accident tolerant (nuclear) fuels (E-ATF) claddings, J. Nucl. Mater. 606 (2025), https://doi.org/10.1016/j.jnucmat.2025.155620.
[35] K. Wei, J. Wei, G. Cao, G. Cheng, W. Li, J. Hu, S. Kano, H. Abe, An interesting oxidation-reduction phenomenon between the Zr(Cr,Fe)2 Laves phase and Cr2O3 under high temperature, Corros. Sci. 246 (2025) 112751, https://doi.org/10.1016/J.CORSCI.2025.112751.
[36] J.C. Brachet, E. Rouesne, J. Ribis, T. Guilbert, S. Urvoy, G. Nony, C. Toffolon-Masclet, M.L. Saux, N. Chaabane, H. Palancher, A. David, J. Bischoff, J. Augereau, E. Pouillier, High temperature steam oxidation of chromium-coated zirconium-based alloys: kinetics and process, Corros. Sci. 167 (2020), https://doi.org/10.1016/j.corsci.2020.108537.
[37] H.M. Chung, T.F. Kassner, Pseudobinary zircaloy-oxygen phase diagram, J. Nucl. Mater. 84 (1979) 327–339, https://doi.org/10.1016/0022-3115(79)90172-7.
[38] D. Kim, M. Ševeček, Y. Lee, Characterization of eutectic reaction of Cr and Cr/CrN coated zircaloy accident tolerant fuel cladding, Nucl. Eng. Technol. 55 (2023) 3535–3542, https://doi.org/10.1016/J.NET.2023.06.015.
[39] M. Steinbrück, Oxidation of zirconium alloys in oxygen at high temperatures up to 1600°C, Oxid. Met. 70 (2008) 317–329, https://doi.org/10.1007/S11085-008-9124-Z.